Passivity-based control of robotic manipulators for safe cooperation with humans

Andrea Maria Zanchettin[a,*], Bakir Lacevic[b] and Paolo Rocco[a]

[a]*Dipartimento di Elettronica, Informazione e Bioingegneria, Politecnico di Milano, Piazza L. Da Vinci 32, 20133, Milano, Italy;*
[b]*Faculty of Electrical Engineering, University of Sarajevo, Obala Kulina bana 7/II, 71000 Sarajevo, Bosnia and Herzegovina*

(*Received 11 September 2013; accepted 17 August 2014*)

1. Introduction

During the last decade, a considerable effort has been taken within the robotics community to bring humans and robots working together or coexisting. Sharing the same space and/or task is a scenario of great relevance for applications ranging from service robotics (Beetz et al., 2001) to co-operative assembly (Wojtara et al., 2009). Regardless of the setting, human safety is the central aspect that unsur-prisingly receives significant attention in both research and engineering practice. Safety in human–robot interaction is usually addressed from the following perspectives: mechan-ical design (intrinsic safety), safety assessment, control and planning.

There are several approaches to enhancing the intrin-sic safety within scenarios where humans and robots can interact. Basic strategies include the design of lightweight manipulators (Hirzinger, Albu-Schäffer, Hahnle, Schaefer, & Sporer, 2001), passive compliant systems and impedance controlled manipulators (Hogan, 1985; Yamada, Hirasawa, Huang, Umetani, & Suita, 1997) or inherently backdrivable manipulators (Salisbury, Townsend, Ebrman, & DiPietro, 1988). Recent solutions are mostly based on a new gen-eration of actuators with variable impedance parameters (Bicchi & Tonietti, 2004; Catalano et al., 2012; Zinn, Khatib, Roth, & Salisbury, 2004) which, however, intro-duces some inherent mechanical compliance.

On the other hand, the concept of safety is usually de-scribed qualitatively, which is sometimes not useful for evaluating the strategies to achieve it (Pervez & Ryu, 2008). Therefore, it is desirable to obtain an unambiguous quanti-tative description of safety. The first attempts for estimat-ing injury risk in human–robot interaction are some well-known indices borrowed from the automotive industry like *Gadd Severity Index* (GSI) (Gadd, 1966) and *Head Injury Criterion* (HIC) (Versace, 1971). However, more elaborated measures, dedicated to robotic applications, have been pro-posed in the literature. In Ikuta, Ishii, and Nokata (2003), the first systematic quantitative method (so-called *danger index*) in safety evaluation, concerning human–robot in-teraction, is presented. Further elaboration of the danger index is carried out in Kulic and Croft (2005) and Kulic and Croft (2006). In Heinzmann and Zelinsky (2003), a quantity called *impact potential* is defined to address the safety assessment problem. Another approach called *danger field* can be found in Lacevic and Rocco (2010). The danger field will be briefly described in Section 2.

From the control perspective, the ubiquitous passivity paradigm has been a very important ingredient within many applications that involve interaction (Albu-Schäffer, Ott, & Hirzinger, 2007; Kugi, Ott, Albu-Schäffer, & Hirzinger, 2008; Lacevic & Rocco, 2011a;Nu˜no, Basa˜nez, & Ortega, 2011). An inherent tendency of passivity-based control to provide compliant motion, (Kazerooni, 1989), makes it a good candidate for scenarios where humans and robots may interact. Furthermore, safety-oriented control that explicitly uses safety measure to improve the safety itself, is of

* Corresponding author. Email: andreamaria.zanchettin@polimi.it

particular interest. Several attempts to address this problem can be found in Kulic and Croft (2006), Lacevic and Rocco (2010), Lacevic and Rocco (2011b), Zanchettin, Lacevic, and Rocco (2012). Though it does not directly use the safety measure, the 'elastic approach' (Brock & Khatib, 2002) is an intuitive method to safety-oriented planning and control. The approach uses so-called *elastic strips/ bands* that are built upon the existing rough global plan for task effectuation. The strips/bands are deformable due to various potentials that are the consequence of obstacles, goal, desired posture, etc. The artificial potential field (Khatib, 1985) may also seem an attractive approach to safety-oriented applications in terms of both real-time control and path planning. The danger assessment can be more or less tied to the values of the repulsive potential.

A disadvantage of this approach is that the classical potential field does not capture the relative motion between the robot and the obstacles unlike in, e.g., Lacevic and Rocco (2010). Another shortcoming is that the potential field method is susceptible of local minima. There have been several attempts to overcome this problem. In Koditschek and Rimon (1990), Rimon and Koditschek (1992), the con-cept of *navigation function* that enables convergence to the destination from almost all initial free configurations is proposed. In De Medio and Oriolo (1991) *vortex fields* are utilised for planning collision-free motions of mobile robots and planar manipulators. In Kim and Khosla (1992), *harmonic potential* is proposed as a tool for local minima-free motion control and planning. *Circulatory fields* (Singh, Stephanou, & Wen, 1996) mimic the magnetic phenom-ena by rotating the robot around the obstacles instead of the usual repulsive action induced by common potential field method. The method is revised in Haddadin, Belder, and Albu-Schaffer (2011) and Haddadin et al. (2010). Other approaches include *vector potential fields* (Masoud & Masoud, 2002), (Masoud, 2010), *artificial coordinating fields* (Jing & Wang, 2004), etc. Despite offering a partial remedy for local minima occurrence, all these methods have a problem whether with lack of guarantee of collision-free motion, or they are impractical for spaces with dimension higher than two.

In this paper, a novel feedback control strategy for robotic manipulators is proposed. The concept of *danger field* has been already exploited from a control perspective in Lacevic, Rocco, and Zanchettin (2013), the sole common denominator with this work being the use of the *danger field* as a quantification of safety during human–robot interaction. Apart from this, the present manuscript proposes a Lyapunov-based control function whereby the motion of the robot is driven by the minimisation of such function, while Lacevic et al. (2013) is based on a more traditional and industrially relevant architecture for velocity control, where the safety action is projected into the null space of a certain production constraint. This paper also presents a theoretical stability analysis, which is only sketched in a simplified scenario in Lacevic et al. (2013). Thanks to the passivity property of the control system proposed in this work, the robot is allowed to come in contact with the environment, which is not allowed in work described in Lacevic et al. (2013). Finally, the validation scenario described in this paper is based on a fixed range camera, rather than on a hand-mounted single beam laser time-of-flight sensor. Moreover, one additional novel contribution of this paper is the guaranteed asymptotic convergence to the workspace-defined goal without getting stuck in local minima.

Preliminary results of this work can be found in Zanchettin et al. (2012). This paper is expanded with further theoretical analysis that includes the proof of convergence in case of moving obstacles. A simple simulation study is included as well. Furthermore, new experiments are presented based on a much more elaborated perception system that includes both visual and force sensors, enabling more realistic validation scenarios.

The remainder of the paper is organised as follows. In Section 2, we briefly recall the so-called danger field, which is used to quantify the level of danger for the robot motion. Section 3 outlines the main contribution of this work and describes the novel passivity-based control law. An illustrative simulation is given in Section 4. Sections 5 and 6 discuss the actual implementation for position-controlled industrial manipulators and present experimental results, respectively. Finally, concluding remarks are given in Section 7.

2. Preliminaries on danger field

In this section, the concept of danger field (Lacevic & Rocco, 2010; Lacevic et al., 2013) is briefly outlined. Basically, the danger field is a scalar quantity that captures how much is a specific state of the robot (position and velocity) dangerous with respect to a generic point in the workspace. The intuition behind is that the danger field decreases with the distance from the robot, whereas it increases with the robot's velocity, particularly if the robot moves towards the location where the field is computed at. Consider first a single point on a robot, located at $\boldsymbol{r}_s \in \mathbb{R}^3$, moving with the velocity $\boldsymbol{v}_s \in \mathbb{R}^3$. The elementary danger field gener-ated by the robot at position $\boldsymbol{r}_j \in \mathbb{R}^3$ could be defined as $DF_e = SDF_e + DDF_e$, where

$$SDF_e = \frac{1}{\epsilon + \|\boldsymbol{r}_j - \boldsymbol{r}_s\|^{\lambda_1}}, \tag{1}$$

$$DDF_e = \|\boldsymbol{v}_s\|^{\lambda_2 - 1} \frac{\|\boldsymbol{r}_j - \boldsymbol{r}_s\| \|\boldsymbol{v}_s\| + \left(\boldsymbol{r}_j - \boldsymbol{r}_s\right)^T \boldsymbol{v}_s}{\epsilon + \|\boldsymbol{r}_j - \boldsymbol{r}_s\|^{\lambda_3 + 1}}, \tag{2}$$

and SDF_e and DDF_e are the elementary static and kinetic danger fields, respectively; $\boldsymbol{v}_s = \boldsymbol{J}_s \dot{\boldsymbol{q}}$, where $\boldsymbol{J}_s$ represents the Jacobian at point $\boldsymbol{r}_s$ on the manipulator and $\dot{\boldsymbol{q}}$ is the

vector of joint velocities, derivatives of suitably defined joint positions $\boldsymbol{q}$; $\epsilon, \lambda_1 \geq 2, \lambda_2 \geq 2, \lambda_3 \geq 1$ are positive parameters.[1] The elementary danger field can be generalised to its cumulative version that captures the position and velocity of the robot's i-th link by performing a path integration along the straight line that represents the wire model of the link[2]:

$$DF = SDF + DDF = \int_0^1 SDF_e(s)ds + \int_0^1 DDF_e(s)ds. \quad (3)$$

Now, for a robot with n links, the cumulative danger field induced at the locations of interest $\boldsymbol{r}_j$, $j = 1, \ldots, n_{\text{obst}}$ (e.g., the relevant positions of obstacles) can be obtained by summing up the contributions of each link and each point.

3. Sensor-based reactive control

In this work, we are interested in developing a state-feedback control law in the form $\boldsymbol{T} = \boldsymbol{T}(\boldsymbol{q}, \dot{\boldsymbol{q}})$, where $\boldsymbol{T}$ is a control input, that stabilises the open-loop dynamics and guarantees the expected safety. In particular, we want the control law to be (a) passivity-based, (b) safety-oriented and (c) to some extent similar to more common state-feedback control laws.

The overall control architecture is sketched in Figure 1. It comprises two blocks: *Workspace sensing* and *Control*. The former is responsible for work-cell supervision and provides information about obstacles (position and geometry), while the latter implements a suitable sensor-based control law. As for the selection of the control law, the main idea is to exploit a PD-like controller with gravity com-pensation, see, e.g. Takegaki and Arimoto (1981a), whose proportional and derivative gains are modified to enforce a safe behaviour of the manipulator.

3.1 *Passivity of danger field*

A first result of this work is the proof of passivity of the danger field, introduced in the previous section. This property will be exploited in the definition of the overall control action.

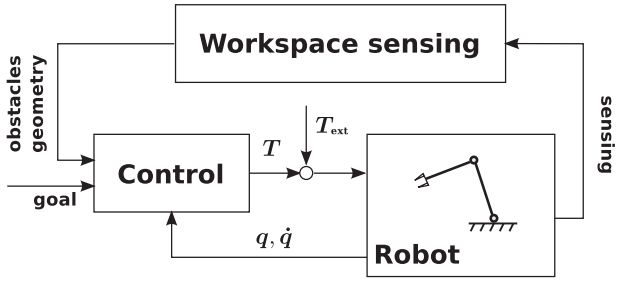

Figure 1. General control architecture.

Theorem 3.1: *Consider the cumulative danger field defined in* (3)*, then the following property holds:*

$$\frac{\partial DF}{\partial \dot{\boldsymbol{q}}}\dot{\boldsymbol{q}} \geq 0, \forall (\boldsymbol{q}, \dot{\boldsymbol{q}}), \quad (4)$$

meaning that $DF(\boldsymbol{q}, \dot{\boldsymbol{q}})$ is a Rayleigh dissipation function, (*Nijmeijer & van der Schaft,* 1990).

Proof: According to Equations (1) and (2), the gradient of the elementary danger field with respect to $\dot{\boldsymbol{q}}$ is given by:

$$\begin{aligned}
&\frac{\partial DF_e}{\partial \dot{\boldsymbol{q}}} \\
&= \frac{\partial SDF_e}{\partial \dot{\boldsymbol{q}}} + \frac{\partial DDF_e}{\partial \dot{\boldsymbol{q}}} = 0 + \frac{\partial DDF_e}{\partial \dot{\boldsymbol{q}}} \\
&= (\lambda_2 - 1)\|\boldsymbol{v}_s\|^{\lambda_2 - 2}\frac{\boldsymbol{v}_s{}^T\boldsymbol{J}_s}{\|\boldsymbol{v}_s\|}\frac{\|\boldsymbol{r}_j - \boldsymbol{r}_s\|\|\boldsymbol{v}_s\|}{\epsilon + \|\boldsymbol{r}_j - \boldsymbol{r}_s\|^{\lambda_3+1}} \\
&\quad + (\lambda_2 - 1)\|\boldsymbol{v}_s\|^{\lambda_2 - 2}\frac{\boldsymbol{v}_s{}^T\boldsymbol{J}_s}{\|\boldsymbol{v}_s\|}\frac{(\boldsymbol{r}_j - \boldsymbol{r}_s)^T\boldsymbol{v}_s}{\epsilon + \|\boldsymbol{r}_j - \boldsymbol{r}_s\|^{\lambda_3+1}} \\
&\quad + \|\boldsymbol{v}_s\|^{\lambda_2 - 2}\frac{\|\boldsymbol{r}_j - \boldsymbol{r}_s\|\boldsymbol{v}_s{}^T\boldsymbol{J}_s + \|\boldsymbol{v}_s\|(\boldsymbol{r}_j - \boldsymbol{r}_s)^T\boldsymbol{J}_s}{\epsilon + \|\boldsymbol{r}_j - \boldsymbol{r}_s\|^{\lambda_3+1}}
\end{aligned} \quad (5)$$

Therefore,[3] since $\boldsymbol{J}_s\dot{\boldsymbol{q}} = \boldsymbol{v}_s$ we observe that

$$\begin{aligned}
\frac{\partial DDF_e}{\partial \dot{\boldsymbol{q}}}\dot{\boldsymbol{q}} &= (\lambda_2 - 1)\|\boldsymbol{v}_s\|^{\lambda_2 - 2}\frac{\boldsymbol{v}_s{}^T\boldsymbol{v}_s}{\|\boldsymbol{v}_s\|} \\
&\quad \times \frac{\|\boldsymbol{r}_j - \boldsymbol{r}_s\|\|\boldsymbol{v}_s\| + (\boldsymbol{r}_j - \boldsymbol{r}_s)^T\boldsymbol{v}_s}{\epsilon + \|\boldsymbol{r}_j - \boldsymbol{r}_s\|^{\lambda_3+1}} \\
&\quad + \|\boldsymbol{v}_s\|^{\lambda_2 - 2}\frac{\|\boldsymbol{r}_j - \boldsymbol{r}_s\|\boldsymbol{v}_s{}^T\boldsymbol{v}_s + \|\boldsymbol{v}_s\|(\boldsymbol{r}_j - \boldsymbol{r}_s)^T\boldsymbol{v}_s}{\epsilon + \|\boldsymbol{r}_j - \boldsymbol{r}_s\|^{\lambda_3+1}} \\
&= \lambda_2\|\boldsymbol{v}_s\|^{\lambda_2 - 1}\frac{\|\boldsymbol{r}_j - \boldsymbol{r}_s\|\|\boldsymbol{v}_s\| + (\boldsymbol{r}_j - \boldsymbol{r}_s)^T\boldsymbol{v}_s}{\epsilon + \|\boldsymbol{r}_j - \boldsymbol{r}_s\|^{\lambda_3+1}} \\
&= \lambda_2 DDF_e \geq 0
\end{aligned} \quad (6)$$

Finally, the elementary quantities can be integrated and summed to obtain the cumulative version, still satisfying

$$\frac{\partial DF}{\partial \dot{\boldsymbol{q}}}\dot{\boldsymbol{q}} = \lambda_2 DDF \geq 0 \quad (7)$$

3.2 *Development of the control law*

In the following, we describe the overall control action and we analytically prove the properties of the closed loop system. Consider the well-known dynamic model of a generic serial-link manipulator:

$$\ddot{\boldsymbol{q}} = \boldsymbol{B}(\boldsymbol{q})^{-1}\left[\boldsymbol{T} - \boldsymbol{h}(\boldsymbol{q}, \dot{\boldsymbol{q}})\dot{\boldsymbol{q}} - \boldsymbol{g}(\boldsymbol{q}) + \boldsymbol{T}_{\text{ext}}\right] \quad (8)$$

where $\boldsymbol{B}(\boldsymbol{q})$ is the positive definite inertia matrix, $\boldsymbol{h}(\boldsymbol{q},\dot{\boldsymbol{q}})\dot{\boldsymbol{q}}$ is the vector of centrifugal/Coriolis terms, $\boldsymbol{g}(\boldsymbol{q})$ is the vector containing gravitational terms, $\boldsymbol{T}$ and $\boldsymbol{T}_{\text{ext}}$ are the vectors of control and external torques[4] applied to the manipulator at the joints, respectively.

The following property of the dynamic model of the manipulator will be used in the proofs:

Proposition 3.2: *There exists a matrix* $\boldsymbol{h}(\boldsymbol{q},\dot{\boldsymbol{q}})$ *such that the matrix* $\dot{\boldsymbol{B}}(\boldsymbol{q}) - 2\boldsymbol{h}(\boldsymbol{q},\dot{\boldsymbol{q}})$ *is skew-symmetric.*

Proof: See Siciliano, Sciavicco, Villani, and Oriolo (2009).

In Theorem 3.1, DF was proved to be a Rayleigh function, so its derivative with respect to joint velocities $\dot{\boldsymbol{q}}$ can be simply adopted as a damping term in the overall control law. The physical meaning of this force/torque is straight-forward: it tries to slow down the motion of the robot in the vicinity of obstacles, while being practically negligible far from them. In fact, as one can see from Equation (5), this damping force/torque is scaled by the distance between the obstacle and the points belonging to the robots, and thus can be neglected as long as the robot does not operate near an obstacle.

As for the P-like part of the controller, we will make use of a scalar artificial potential function $U(\boldsymbol{q})$ which has a global minimum in the goal configuration, e.g., a quadratic function of the error as in Khatib (1985). The main difficulty here is in the selection of a potential suitable to drive the robot from any initial configuration to the final config-uration without introducing local minima in the definition of the overall potential field, see, e.g., Koditschek (1987).

The problem can thus be expressed as follows: define a control action depending on the attractive potential field U and on the danger field DF which steers the robot towards the goal position, while avoiding collision with obstacles, and such that the asymptotic accomplishment of the positioning task is *guaranteed*.

The overall control action is computed by the superposition of the attractive and obstacle-related terms and by adding the gravity compensation, yielding

$$\begin{aligned}\boldsymbol{T} = &-\gamma(\nabla U)^T - \alpha(\boldsymbol{q})\boldsymbol{P}_\perp(\dot{\boldsymbol{q}})(\nabla SDF)^T \\ &- \boldsymbol{K}_D\dot{\boldsymbol{q}} - \beta(\boldsymbol{q},\dot{\boldsymbol{q}})\left(\frac{\partial DF}{\partial\dot{\boldsymbol{q}}}\right)^T + \boldsymbol{g}(\boldsymbol{q})\end{aligned} \tag{9}$$

where $\gamma > 0$ is a scalar parameter,

$$\boldsymbol{P}_\perp(\dot{\boldsymbol{q}}) = \|\dot{\boldsymbol{q}}\|^2\boldsymbol{I}_n - \dot{\boldsymbol{q}}\dot{\boldsymbol{q}}^T$$

is a projection matrix, $\boldsymbol{I}_n$ is the $n\times n$ identity matrix, $\boldsymbol{K}_D = \boldsymbol{K}_D^T > 0$ is a matrix of joint dampings (i.e. the derivative gains), and functions $\alpha(\boldsymbol{q}) \geq 0$ and $\beta(\boldsymbol{q},\dot{\boldsymbol{q}}) \geq 0$ represent scalar (possibly configuration- or velocity-dependent) positive and bounded scaling factors.

3.3 *Passivity of the closed-loop system*

Theorem 3.3: *The closed-loop system* (8)–(9) *enforces a passive mapping between* $\boldsymbol{T}_{ext}$ *and* $\dot{\boldsymbol{q}}$.

Proof: Consider the following candidate storage function:

$$V(\boldsymbol{q},\dot{\boldsymbol{q}}) = \gamma U(\boldsymbol{q}) + \frac{1}{2}\dot{\boldsymbol{q}}^T\boldsymbol{B}(\boldsymbol{q})\dot{\boldsymbol{q}} \tag{10}$$

then, its derivative along the trajectories of the system is

$$\begin{aligned}\dot{V} &= \gamma\nabla U\dot{\boldsymbol{q}} + \dot{\boldsymbol{q}}^T\boldsymbol{B}(\boldsymbol{q})\ddot{\boldsymbol{q}} + \frac{1}{2}\dot{\boldsymbol{q}}^T\dot{\boldsymbol{B}}(\boldsymbol{q})\dot{\boldsymbol{q}} \\ &= \gamma\nabla U\dot{\boldsymbol{q}} + \dot{\boldsymbol{q}}^T\boldsymbol{T} - \dot{\boldsymbol{q}}^T\boldsymbol{h}(\boldsymbol{q},\dot{\boldsymbol{q}})\dot{\boldsymbol{q}} - \dot{\boldsymbol{q}}^T\boldsymbol{g}(\boldsymbol{q}) \\ &\quad + \dot{\boldsymbol{q}}^T\boldsymbol{T}_{ext} + \frac{1}{2}\dot{\boldsymbol{q}}^T\dot{\boldsymbol{B}}(\boldsymbol{q})\dot{\boldsymbol{q}} \\ &= \gamma\nabla U\dot{\boldsymbol{q}} + \dot{\boldsymbol{q}}^T\boldsymbol{T} + \frac{1}{2}\dot{\boldsymbol{q}}^T\left(\dot{\boldsymbol{B}}(\boldsymbol{q}) - 2\boldsymbol{h}(\boldsymbol{q},\dot{\boldsymbol{q}})\right)\dot{\boldsymbol{q}} \\ &\quad - \dot{\boldsymbol{q}}^T\boldsymbol{g}(\boldsymbol{q}) + \dot{\boldsymbol{q}}^T\boldsymbol{T}_{ext}\end{aligned} \tag{11}$$

Substituting the control law (9) in (11) and using Proposition 3.2, from the definition of matrix $\boldsymbol{P}_\perp(\cdot)$ we obtain

$$\begin{aligned}\dot{V} &= -\dot{\boldsymbol{q}}^T\alpha(\boldsymbol{q})\boldsymbol{P}_\perp(\dot{\boldsymbol{q}})(\nabla SDF)^T \\ &\quad - \dot{\boldsymbol{q}}^T\boldsymbol{K}_D\dot{\boldsymbol{q}} - \beta(\boldsymbol{q},\dot{\boldsymbol{q}})\frac{\partial DF}{\partial\dot{\boldsymbol{q}}}\dot{\boldsymbol{q}} + \dot{\boldsymbol{q}}^T\boldsymbol{T}_{ext} \\ &= -\beta(\boldsymbol{q},\dot{\boldsymbol{q}})\lambda_2 DDF - \dot{\boldsymbol{q}}^T\boldsymbol{K}_D\dot{\boldsymbol{q}} + \dot{\boldsymbol{q}}^T\boldsymbol{T}_{ext}\end{aligned} \tag{12}$$

As a consequence of Theorem 3.1 and the nature of the projection matrix, we finally obtain $\dot{V} \leq \dot{\boldsymbol{q}}^T\boldsymbol{T}_{ext}$ which proves the passivity of the mapping between $\boldsymbol{T}_{ext}$ and $\dot{\boldsymbol{q}}$.

Remark 1: Theorem 3.3 proves the passivity of the mapping from $\boldsymbol{T}_{ext}$ to $\dot{\boldsymbol{q}}$, meaning that at any time the energy stored in the system is bounded from above, even when the system exchanges energy with the environment, e.g., due to contact forces. In other words, the following inequality holds:

$$V(t) - V(t_0) \leq \int_{t_0}^{t}\dot{\boldsymbol{q}}^T\boldsymbol{T}_{ext}d\tau \tag{13}$$

for any $t \geq t_0$. Thus, the instantaneous variation of the stored energy $V(t) - V(t_0)$ is always less or equal to the energy introduced in the system from the environment.

3.4 *Stability with moving obstacles*

For fixed obstacles and when $\boldsymbol{T}_{ext} = \boldsymbol{0}$, the asymptotic stability of the goal position is a direct consequence of the Barbashin–Krasovskii invariant principle, see, e.g., Khalil (2002). In case of moving obstacles, however, the situation is more involved. In fact, the danger field is computed along these moving obstacles and then adopted within the control

law (9). It follows that the overall closed-loop system becomes non-autonomous. In the following, we prove that the controller guarantees the accomplishment of the positioning task, even in this situation, without incurring in local minima.

Corollary 3.4: *Assume* $\boldsymbol{T}_{ext} = \mathbf{0}$*, at least ultimately, then the goal position of the closed-loop system* (8)–(9) *is uniformly asymptotically stable in the basin of attraction of* U.

Proof: In case $\boldsymbol{T}_{ext} = \mathbf{0}$, we have already proved that $\dot{V}(\boldsymbol{q}, \dot{\boldsymbol{q}}, t) \leq 0$. Notice that since the candidate Lyapunov function is time-independent, it follows that the goal position is uniformly stable. In fact, one can easily find $W_1(\boldsymbol{q}, \dot{\boldsymbol{q}})$, $W_2(\boldsymbol{q}, \dot{\boldsymbol{q}}) > 0$ such that[5]

$$W_1(\boldsymbol{q}, \dot{\boldsymbol{q}}) \leq V(\boldsymbol{q}, \dot{\boldsymbol{q}}) \leq W_2(\boldsymbol{q}, \dot{\boldsymbol{q}})$$

hence $V(t)$ approaches a finite positive limit, say $V_\infty \geq 0$, as $t \to \infty$. Notice that there exists a function $W_3(\boldsymbol{q}, \dot{\boldsymbol{q}}) \geq 0$ such that

$$\dot{V}(\boldsymbol{q}, \dot{\boldsymbol{q}}, t) = -\beta(\boldsymbol{q}, \dot{\boldsymbol{q}}) \lambda_2 DDF - \dot{\boldsymbol{q}}^T \boldsymbol{K}_D \dot{\boldsymbol{q}} \tag{14}$$

and $\dot{V} \leq -W_3(\boldsymbol{q}, \dot{\boldsymbol{q}}) = -\dot{\boldsymbol{q}}^T \boldsymbol{K}_D \dot{\boldsymbol{q}}$, where W_3 is uniformly continuous in time, being $\ddot{\boldsymbol{q}}$ bounded.[6] Moreover

$$\int_{t_0}^{\infty} W_3(t)\, dt \leq -\int_{t_0}^{\infty} \dot{V}(t)\, dt = V(t_0) - V_\infty \tag{15}$$

is finite and bounded. Therefore, by application of the Barbalat lemma, see, e.g., Khalil (2002), it follows that W_3 approaches 0 as $t \to \infty$. This means that, since $\boldsymbol{K}_D > 0$, $\dot{\boldsymbol{q}}$ will also approach zero as $t \to \infty$.

This situation implies that the state of the system will approach the largest positive limit set such that $W_3 = 0$, see Khalil (2002), hence $\dot{\boldsymbol{q}} = \ddot{\boldsymbol{q}} = \mathbf{0}$ and therefore $\boldsymbol{T} = \boldsymbol{g}(\boldsymbol{q})$. On the other hand, this implies $\nabla U = \mathbf{0}^T$ and finally $U = 0$, meaning that the largest positive invariant set contained in $W_3 = 0$ is the goal position.

Remark 2: Corollary 3.4 discusses the uniform asymptotic stability of the goal position in case of moving obstacles. In this situation, in fact, the passivity of the system is still preserved, however, the asymptotic convergence of the Lyapunov function in Equation (10) to zero is not straight-forward. By exploiting the Barbalat lemma, we have been able to show that the robot under the proposed control law is able to asymptotically reach the goal position, without incurring in local minima.

Remark 3: The control law proposed in Equation (9) has been obtained by the superposition of attractive and repulsive control actions. While the former is needed to steer the robot towards the goal position, the latter attempts to maintain the robot itself away from the perceived workspace obstacles. Differently from other approaches, like the arti-ficial potential fields in Khatib (1985) or Koditschek and Rimon (1990), the composition of the two, possibly conflicting, actions is not addressed by direct sum or a more elaborated combination of the two components. Whilst the goal-dependent potential U has been introduced in a standard way, see, e.g., Takegaki and Arimoto (1981b), and appears in the Lyapunov function, the repulsive action, here represented by the danger field, has been included in such a way to introduce a passive action, as proved in Theorem 3.1. Notice that the danger field does not appear in the Lyapunov function. Contrarily to standard approaches based on attractive and repulsive artificial potential fields, which are susceptible of local minima, the use of the danger field is here designed so as not to interfere with the positioning task. This results, as proved in Corollary 3.4, is the uniform asymptotic stability of the goal position in the basin of attraction of U, without incurring in local minima.

4. A simulated case study

In the following, the control strategy presented in Section 3 is applied to a case study involving a 2-dof planar manipulator in the horizontal plane described by the following dynamic model:

$$\begin{aligned} \boldsymbol{B}(\boldsymbol{q}) &= \begin{bmatrix} 1/6 + 1.5\cos(q_2) & 1/3 + 0.5\cos(q_2) \\ 1/3 + 0.5\cos(q_2) & 1/3 \end{bmatrix} \\ \boldsymbol{h}(\boldsymbol{q}, \dot{\boldsymbol{q}}) &= \begin{bmatrix} -0.5\sin(q_2)\dot{q}_2 & -0.5\sin(q_2)(\dot{q}_1 + \dot{q}_2) \\ 0.5\sin(q_2)\dot{q}_1 & 0 \end{bmatrix} \end{aligned} \tag{16}$$

corresponding to 1 m length links of 1 kg, regarded as thin rods with uniformly distributed mass. Despite the seeming simplicity, the problem of finding a collision-free trajectory in a 2D space is even more involved than in a 3D space. Planar motion, in fact, reduces the chances of computing evasive motion for the robot to circumvent obstacles. For a positioning task in the Cartesian space, the following attractive potential has been selected

$$U = \frac{1}{2} \frac{\|\boldsymbol{e}\|^2}{\|\boldsymbol{e}\|^2 + 1}$$

where $\boldsymbol{e} = \boldsymbol{x}^d - \boldsymbol{x}(\boldsymbol{q})$ is the Cartesian error between the desired and the actual positions of the end-effector. According to the methodology described in this paper, the control torque in Equation (9) (except for the gravitational effect) has been used, where $\gamma = 10$, $\boldsymbol{K}_D = 10\boldsymbol{I}_2$, $\alpha(\boldsymbol{q}) = \beta(\boldsymbol{q}, \dot{\boldsymbol{q}}) = 5$, $\lambda_1 = \lambda_2 = 2$, $\lambda_3 = 1$ have been selected.

To verify the avoidance of local minima, a set of obstacles is arranged around the robot as in Figure 2(b). Because of the geometry of the obstacles, standard approaches involving repulsive fields, see, e.g., Khatib (1985), might fail due to the occurrence of undesirable local min-ima. Figure 2(a) reports the time history of the Lyapunov

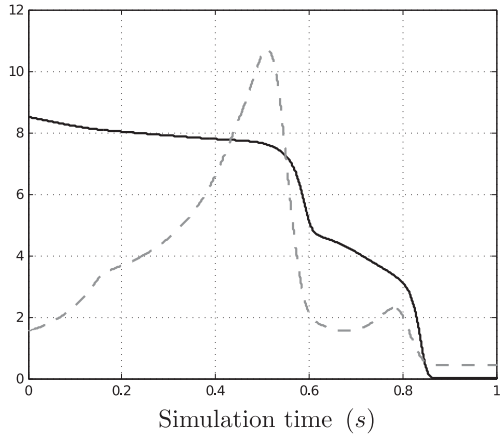

(a) Lyapunov function (solid) and (x0.1, scaled danger field (dashed gray)

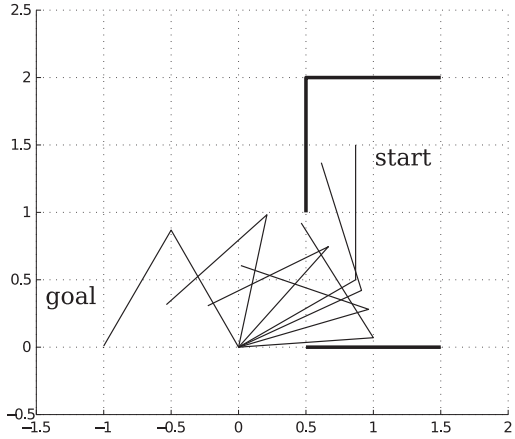

(b) Computed trajectory in presence of concave obstacles

Figure 2. Lyapunov function, danger field and computed path.

function in Equation (10) and the profile of the danger field. As one can see, the Lyapunov function (regarded as a func-tion of time) tends to zero, consistent with Corollary 3.4, confirming that the controller can reach the goal position without incurring in local minima. Moreover, the sequence of configurations adopted by the manipulator to avoid the obstacles are shown in Figure 2(b). As a final verification, Figure 3 shows the computed path (dashed line) in the con-figuration space using the proposed approach. The path is compared with the contour plot obtained applying the artificial potential method with a FIRAS-like[7] repulsive function

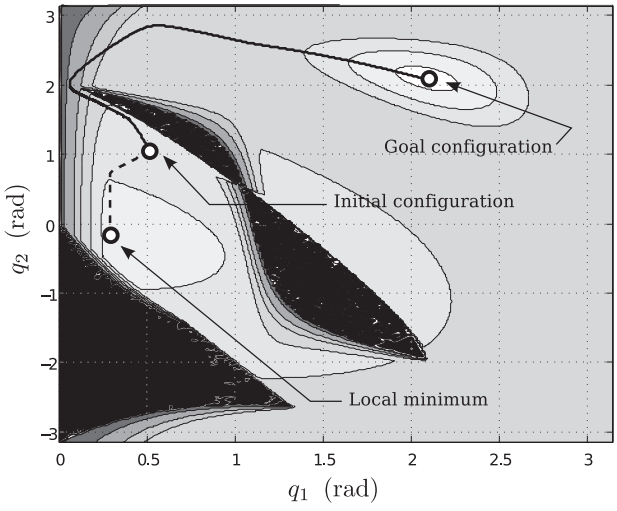

Figure 3. Path computed with the proposed approach (solid black) compared with the one following the steepest descent algorithm (dashed black) and contour plot of the artificial potential, obtained combining the attractive and a repulsive field; black areas represent obstacles in the configuration space.

defined as follows

$$U_{\text{rep}}(\boldsymbol{q}) = \begin{cases} \sum_{j=1}^{n_{\text{obst}}} \left(SDF_j - SDF_t\right)^2, & \text{if } SDF_j \geq SDF_t \\ 0, & \text{otherwise} \end{cases} \tag{17}$$

where SDF_j is the danger field induced by the robot and computed in an obstacle location, while SDF_t is a predefined threshold. The value of U_{rep} has its maximum as the robot approaches the obstacle's surface, but its influence is limited to a given region surrounding the obstacle itself, such that $SDF \geq SDF_t = 5$. As one can see, even in this simple case the adoption of a standard artificial potential incurs in local minima, while the proposed approach is able to steer the robot from the initial to the final configuration. Moreover, the adoption of the danger field in forming the control action helps in reducing the speed when the robot is close to the obstacle surface. This is particularly clear during the first part of the simulation, i.e. approximately from time $t = 0$ to time $t \approx 0.5\ s$, where the velocity of the robot is particularly low as emphasised by the reduced, though negative, slope of the Lyapunov function in Figure 2(a).

5. Implementation

Assume that the positioning task can be described in terms of position and orientation and a unit quaternion has been selected to describe the desired orientation. Therefore, the goal position is identified by vector $\boldsymbol{v}^d = \left[\, x_d \;\; y_d \;\; z_d \;\; \eta_d \;\; \boldsymbol{\epsilon}_d{}^T \,\right]^T$ where x_d, y_d and z_d stand for desired Cartesian coordinates while η_d and $\boldsymbol{\epsilon}_d$ are the scalar and vector parts of a unit quaternion, respectively. The

following attractive potential field can be then selected[8]:

$$U = \frac{1}{2}\frac{\boldsymbol{e}^T \boldsymbol{K} \boldsymbol{e}}{\boldsymbol{e}^T \boldsymbol{K} \boldsymbol{e} + \zeta}, \quad \boldsymbol{e} = \boldsymbol{v}^d - \boldsymbol{v}(\boldsymbol{q}) \tag{18}$$

where $0 < \zeta \leq 1$ and $\boldsymbol{K} = \text{blkdiag}\left(k_p \boldsymbol{I}_3, k_o \boldsymbol{I}_4\right) = \boldsymbol{K}^{\mathrm{T}} > 0$, $k_p > 0$, $k_o > 0$. Using the quaternion propagation law, see e.g. Siciliano et al. (2009), it can be verified that

$$-(\nabla U)^T = \frac{\zeta \boldsymbol{J}^T}{\left(\boldsymbol{e}^T \boldsymbol{K} \boldsymbol{e} + \zeta\right)^2} \begin{bmatrix} k_p \boldsymbol{I}_3 & 0 \\ 0 & \frac{k_o}{2} \boldsymbol{I}_3 \end{bmatrix} \begin{bmatrix} \boldsymbol{e}_p \\ \boldsymbol{e}_o \end{bmatrix} \tag{19}$$

where $\boldsymbol{J}$ is the geometrical Jacobian of the manipulator, $\boldsymbol{e}_p$ is the error in the Cartesian coordinates, while $\boldsymbol{e}_o = \eta \boldsymbol{\epsilon}_d - \eta_d \boldsymbol{\epsilon} + \boldsymbol{\epsilon} \times \boldsymbol{\epsilon}_d$.

When it comes to implement the controller on an industrial manipulator, the approach described so far is hardly applicable due to the limited accessibility of industrial controllers. Therefore, we implemented the controller on top of the existing position/velocity loops, as sketched in Figure 4. This approach guarantees a more robust steady-state performance, e.g. to compensate the gravitational load. However, in case of physical human–robot interaction, the backdrivability of the robot in the presence of external forces is compromised. The use of a force/torque sensor is thus required and implies a modification of the control law in Equation (9), yielding

$$\ddot{\boldsymbol{q}} = \boldsymbol{J}^T \boldsymbol{h}_{ext} + \frac{\gamma \zeta \boldsymbol{J}^T}{\left(\boldsymbol{e}^T \boldsymbol{K} \boldsymbol{e} + \zeta\right)^2} \begin{bmatrix} k_p \boldsymbol{I}_3 & 0 \\ 0 & \frac{k_o}{2} \boldsymbol{I}_3 \end{bmatrix} \begin{bmatrix} \boldsymbol{e}_p \\ \boldsymbol{e}_o \end{bmatrix} - \boldsymbol{K}_D \dot{\boldsymbol{q}} - \alpha(\boldsymbol{q}) \boldsymbol{P}_{\perp}(\dot{\boldsymbol{q}}) (\nabla SDF)^T - \beta(\boldsymbol{q}, \dot{\boldsymbol{q}}) \left(\frac{\partial DF}{\partial \dot{\boldsymbol{q}}}\right)^T \tag{20}$$

where $\boldsymbol{h}_{ext}$ is the end-effector force/moment measured by the wrist mounted sensor. Equation (20) is integrated within the controller and its outputs $\boldsymbol{q}, \dot{\boldsymbol{q}}$ are sent as references to the inner position/velocity loops (see Figure 4).

Remark 4: Notice that Equation (20) inherits the same stability-related properties of Equations (8)–(9), once adopted to control a double integrator system, rather than the real system dynamics in Equation (8), or equivalently, once interfaced with a mechanical system with $\boldsymbol{B}(\boldsymbol{q}) = \boldsymbol{I}$ and $\boldsymbol{g}(\boldsymbol{q}) = \boldsymbol{0}$ where the external disturbance torque $\boldsymbol{T}_{ext}$ has been compensated by the lower-level controller. This is the case, for example, of the adoption of a feedback linearising low-level controller, see e.g. Tarn, Bejczy, Isidori, and Chen (1984).

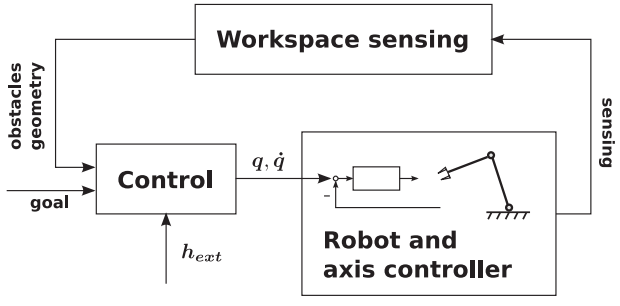

Figure 4. Control architecture for position controlled robot.

6. Experiments

As a validation of the proposed control strategy, experimental tests have been carried out on an industrial manipulator. The six axes ABB IRB-140 robot with 6 kg payload was used for this purpose. The manipulator is equipped with an ATI force/torque sensor mounted on the robot end-effector and interfaced to the controller with a real-time communication link, see Blomdell, Dressler, Nilsson, and Robertsson (2010). The operator, regarded as a moving obstacle, is able at any time to enter the working range of the robot for inspection. For this reason, a proper safety action should be guaranteed, possibly without interrupting the production. For workspace surveillance, a range camera (MICROSOFT KINECT) with the OPENNI drivers has been selected. The output of the sensor consists of a segment representation of the human silhouette capturing the position of anatomical points along the body (head, shoulder, elbow, wrist, hip, etc.). The danger field in Equation (3) together with its derivatives are computed along the selected points on the body parts (i.e. one point on each upper arm and forearm, one point on the torso and one on the head) and then forwarded to the state-feedback controller. A 4 ms discrete-time implementation of the control law in Equation (20) is then computed and its output (position and velocity references) is then propagated to the low-level axis controller.

The following parameters have been selected for the control law in Equation (20): $\lambda_1 = \lambda_2 = 2, \lambda_3 = 1, \gamma = 200, k_p = 0.5, k_o = 1, \zeta = 0.1, \boldsymbol{K}_D = 40\boldsymbol{I}_6$. Parameters γ and $\boldsymbol{K}_D$ have been selected to obtain a reasonable duration of the positioning task, while ζ has been tuned to speed up the final asymptotic convergence to the desired configuration. As for the weighting factors α and β, we selected $\alpha(\boldsymbol{q}) = 0.5SDF$ and $\beta(\boldsymbol{q}, \dot{\boldsymbol{q}}) = 0.5DF$ to fully integrate the danger-field in the control action. In fact, from Equation (20), it is clear that the desired robot acceleration $\ddot{\boldsymbol{q}}$ depends on the derivatives of the danger-field only. In this way, the robot motion profile depends also on the danger field itself, possibly making the obstacle avoidance more effective.

During the experiment, the same production cycle, consisting of moving back and forth between two points (one above the table at position $x_1 = 0.5\,\text{m}$, $y_1 = -0.4\,\text{m}$, $z_1 = 0.2\,\text{m}$ and the other one sideways, $x_2 = 0.5\,\text{m}$, $y_2 = 0.2\,\text{m}$, $z_2 = 0.2\,\text{m}$), has been repeated four times. However, during the second and third

repetitions, the human operator is within the working range of the robot, see Figures 5(b) and 5(c). At time instant $t \approx 7$ s (approximately at the beginning of the second cy-cle), he walked towards the robot and finally abandoned the robot's working area at time instant $t \approx 33$ s (approxi-mately at the end of the third cycle). This is confirmed by the profile of the danger field, see Figure 6, which captured a more dangerous situation due to the vicinity of the human. Correspondingly, the robot first tries to reduce the speed and take a different path (see e.g. in Figure 7 the different x-coordinate around time instants $t \approx 6$ s and $t \approx 18$ s) to reach the goal configuration. Figures 7 and 8 report the time histories of the tool position and of the sensed force, respectively, during the experiment. Notice that during the two repetitions performed with a human (and highlighted in Figure 7), the task has been performed more slowly. At the beginning of the third repetition, the human oper-ator positioned a balloon on the table (see Figure 5(c)), corresponding to one of the positions reached by the robot during the task. Therefore, during the last two repetitions, the robot came in contact with a soft (passive) environment and adjusted the tool position according to the

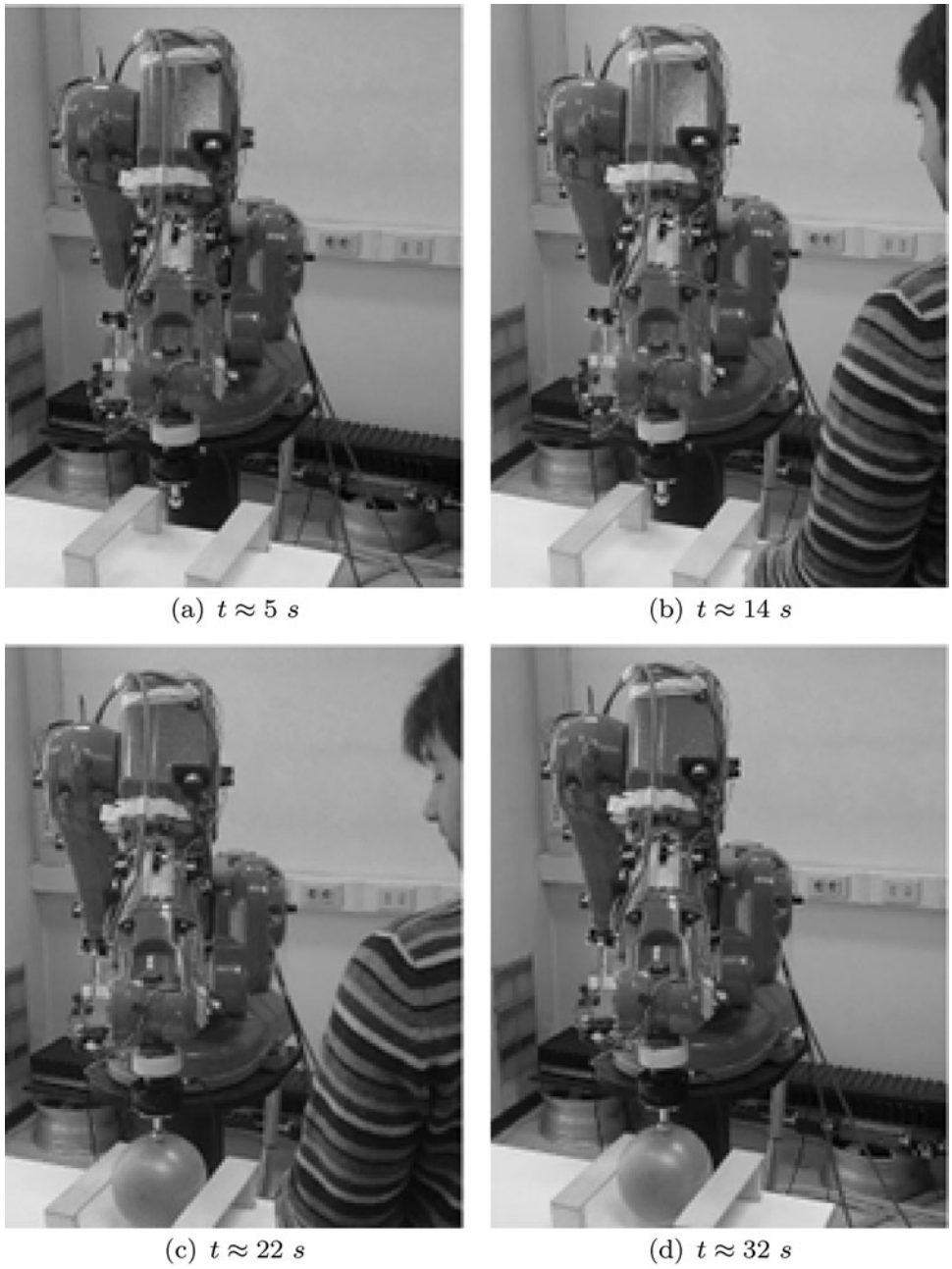

(a) $t \approx 5\ s$ (b) $t \approx 14\ s$

(c) $t \approx 22\ s$ (d) $t \approx 32\ s$

Figure 5. Robot positions along the experiments.

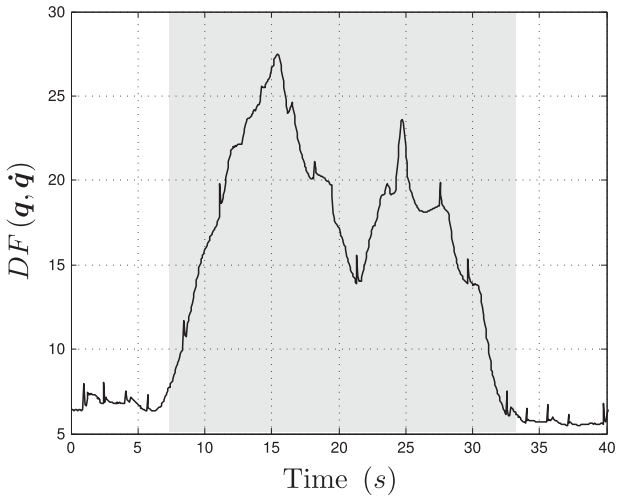

Figure 6. Danger Field induced by the robot on the human operator.

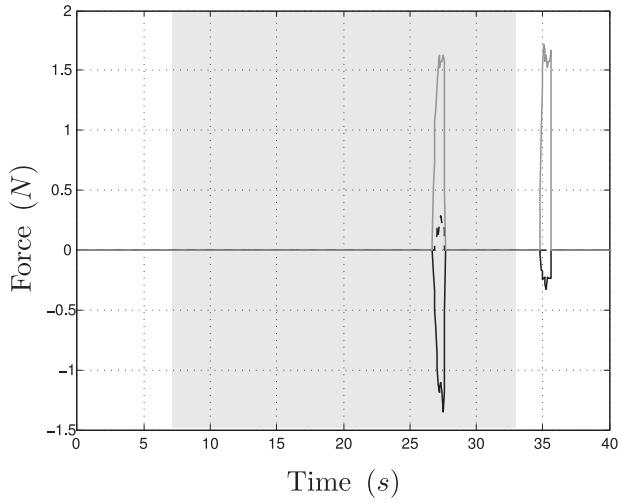

Figure 8. Measured forces in world frame (F_x solid black, F_y dashed black, F_z solid gray).

measured force. Moreover during the third repetition the robot was still operating at a reduced speed. During the last cycle, instead, since the operator was leaving the workspace of the robot, see Figure 5(d), the robot could operate at higher speed, still maintaining a compliant reaction to contact forces. Notice that during the last two repetitions, the goal position is not reached (see Figure 7 at approximately time $t = 27$ s and $t = 35$ s) due to the presence of contact forces, as shown in Figure 8.

The accompanying video[9] complements the description of the developed control strategy by showing the obstacle avoidance capabilities of the robot during a reaching task, its velocity adaptation due to the vicinity of obstacles as well as the trajectory adaptation in response to a sensed force.

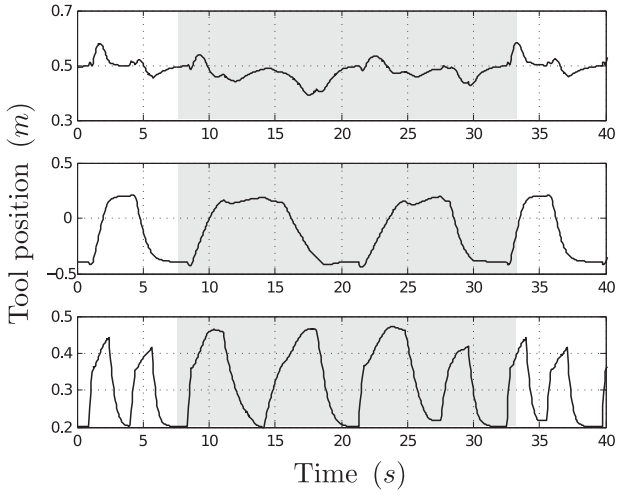

Figure 7. Tool Cartesian position in world frame (from top x, y, z).

7. Conclusions

This paper presented a newly conceived passivity-based control scheme for robotic manipulators for safe cooperation with humans. The main contribution of this work is the development of a control law that guarantees the achievement of a position/orientation goal in an environment populated by obstacles, while not incurring in local minima. The control law has been verified by simulating a case study showing the possibility to move the robot towards the goal position in case of concave obstacles. Moreover, an experimental verification has been provided, involving an industrial manipulator operating in a workspace without physical barriers, that also humans can access with guaranteed safety.

Funding

The research leading to these results has received funding from the European Community's Seventh Framework Programme FP7/2007-2013 Challenge 2 – Cognitive Systems, Interaction, Robotics [grant number 230902; project ROSETTA].

Supplemental data

An accompanying video complementing the description of the developed control strategy by showing the avoidance capability of the robot during a reaching task can be accessed here.

Notes

1. Note that this is a slight generalisation of the danger field with respect to Lacevic and Rocco (2010).
2. The dependency on s of both the SDF_e and the DDF_e is in all the quantities in (1) and (2) having subscript $\boldsymbol{s}$, which are affine functions of s.
3. Notice that $\partial DF_e/\partial\dot{\boldsymbol{q}}$ can be defined for continuity to be zero for $\boldsymbol{v}_s = \boldsymbol{0}$.

4. Depending on the nature of the joint (prismatic or rotational) the related component of $\boldsymbol{T}$ and $\boldsymbol{T}_{\text{ext}}$ is a torque or a force.
5. For example, one could select $W_1 = (1 - a)\, V$ and $W_2 = (1 + a)\, V$ where $0 < a < 1$.
6. This is a consequence of the passivity of the closed-loop system and, from the definition of *DF*in (3), of the boundedness of the control signal.
7. Artificial Repulsion from the Surface of the obstacle (FIRAS, from French), (Khatib, 1985).
8. Such a function has been designed to avoid fast motions to due large errors, which can be introduced by using, e.g. $\boldsymbol{e}^T \boldsymbol{K} \boldsymbol{e}$.
9. See also http://www.youtube.com/watch?v=yXSdurZ82FM.

References

Albu-Schäffer, A., Ott, C., & Hirzinger, G. (2007). A unified passivity-based control framework for position, torque and impedance control of flexible joint robots. *International Journal of Robotic Research, 26*, 23–39.

Beetz, M., Arbuckle, T., Belker, T., Bennewitz, M., Burgard, W., Cremers, A.B., . . .Schulz, D. (2001). Integrated plan-based control of autonomous service robots in human environments. *IEEE Intelligent Systems, 16*, 56–65.

Bicchi, A., & Tonietti, G. (2004). Fast and soft-arm tactics [robot arm design]. *Robotics Automation Magazine, IEEE, 11*, 22–33.

Blomdell, A., Dressler, I., Nilsson, K., & Robertsson, A. (2010). Flexible application development and high-performance motion control based on external sensing and reconfiguration of ABB industrial robot controllers. *Workshop on innovative robot control architectures for semanding (research) applications*. Anchorage, AK.

Brock, O., & Khatib, O. (2002). Elastic strips: A framework for motion generation in human environments. *International Journal of Robotics Research, 21*, 1031–1052.

Catalano, M., Grioli, G., Garabini, M., Belo, F., Di Basco, A., Tsagarakis, N., & Bicchi, A. (2012). A variable damping module for variable impedance actuation. *International conference of robotics and automation, ICRA* (pp. 2666–2672). New York, NY: IEEE.

De Medio, C., & Oriolo, G. (1991). Robot obstacle avoidance using vortex fields. In S. Stifter & J. Lenarcic (Eds.), *Advances in robot kinematics* (pp. 227–235). Wien, Austria: Springer-Verlag.

Gadd, C.W. (1966). Use of weighted-impulse criterion for estimating injury hazard. *Car crash conference* (pp. 164–174). Warrendale, PA: Society of Automotive Engineers.

Haddadin, S., Belder, R., & Albu-Schaffer, A. (2011). Dynamic motion planning for robots in partially unknown environments. *IFAC world congress* (pp. 6842–6850). Milano, Italy: IFAC.

Haddadin, S., Urbanek, H., Parusel, S., Burschka, D., Rossmann, J., Albu-Schaffer, A., & Hirzinger, G. (2010). Real-time reactive motion generation based on variable attractor dynamics and shaped velocities. *IEEE/RSJ international conference on intelligent robots and systems, IROS* (pp. 3109–3116). New York, NY: IEEE.

Heinzmann, J., & Zelinsky, A. (2003). Quantitative safety guarantees for physical human-robot interaction. *International Journal of Robotics Research, 22*, 479–504.

Hirzinger, G., Albu-Schäffer, A., Hahnle, M., Schaefer, I., & Sporer, N. (2001). On a new generation of torque controlled light-weight robots. *IEEE international conference on robotics and automation, ICRA* (pp. 3356–3363). New York, NY: IEEE.

Hogan, N. (1985). Impedance control: An approach to manipulation: Part III-applications. *ASME Journal of Dynamic Systems Measurement and Control*, *107*, 17–24.

Ikuta, K., Ishii, H., & Nokata, M. (2003). Safety evaluation method of design and control for human-care robots. *International Journal of Robotics Research, 22*, 281–298.

Jing, X., & Wang, Y. (2004). Local minima-free design of artificial coordinating fields. *Journal of Control Theory and Applications, 2*, 371–380.

Kazerooni, H. (1989). Compliant motion control for robot manipulators. *International Journal of Control, 49*, 745–760.

Khalil, H.K. (2002). *Nonlinear systems*. Prentice Hall.

Khatib, O. (1985). Real-time obstacle avoidance for manipulators and mobile robots. *IEEE International conference on robotics and automation, ICRA* (pp. 500–505). New York, NY: IEEE.

Kim, J., & Khosla, P. (1992). Real-time obstacle avoidance using harmonic potential functions. *IEEE Transactions on Robotics and Automation, 8*, 338–349.

Koditschek, D. (1987). Exact robot navigation by means of potential functions: Some topological considerations. *IEEE international conference on robotics and automation, ICRA* (pp. 412–442). Netherlands: Elsevier.

Koditschek, D., & Rimon, E. (1990). Robot navigation functions on manifolds with boundary. *Advanced Applied Mathematics, 11*, 412–442.

Kugi, A., Ott, C., Albu-Schäffer, A., & Hirzinger, G. (2008). On the passivity-based impedance control of flexible joint robots. *IEEE Transactions on Robotics, 24*, 416–429.

Kulic, D., & Croft, E.A. (2005). Safe planning for human-robot interaction. *Journal of Robotic Systems, 22*, 383–396.

Kulic, D., & Croft, E.A. (2006). Real-time safety for human-robot interaction. *Robotics and Autonomous Systems, 54*, 1–12.

Lacevic, B., & Rocco, P. (2010). Kinetostatic danger field - A novel safety assessment for human-robot interaction. *IEEE/RSJ international conference on intelligent robots and systems, IROS* (pp. 2169–2174). New York, NY: IEEE.

Lacevic, B., & Rocco, P. (2011a). Closed form solution to controller design for human-robot interaction. *ASME Journal of Dynamic Systems, Measurement, and Control*, *133*(2).

Lacevic, B., & Rocco, P. (2011b). Safety-oriented control of robotic manipulators - A kinematic approach. *IFAC world congress* (pp. 11508–11513). Milano, Italy: IFAC.

Lacevic, B., Rocco, P., & Zanchettin, A. (2013). Safety assessment and control of robotic manipulators using danger field. *IEEE Transactions on Robotics*, available online.

Masoud, A. (2010). Kinodynamic motion planning: A novel type of nonlinear, passive damping forces and advantages. *IEEE Robotics and Automation Magazine, 17*, 85–99.

Masoud, S., & Masoud, A. (2002). Motion planning in the presence of directional and regional avoidance constraints using nonlinear, anisotropic, harmonic potential fields: A physical metaphor. *IEEE Transactions on Systems, Man and Cybernetics, Part A: Systems and Humans, 32*, 705–723.

Nijmeijer, H., & van der Schaft, A.J. (1990). *Nonlinear dynamical control systems*. New York, NY: Springer.

Nuño, E., Basañez, L., & Ortega, R. (2011). Passivity-based control for bilateral teleoperation: A tutorial. *Automatica, 47*, 485–495.

Pervez, A., & Ryu, J. (2008). Safe physical human robot interaction-past, present and future. *Journal of Mechanical Science and Technology, 22*, 469–483.

Rimon, E., & Koditschek, D. (1992). Exact robot navigation using artificial potential functions. *IEEE Transactions on Robotics and Automation, 8*, 501–518.

Salisbury, K., Townsend, W., Ebrman, B., & DiPietro, D. (1988). Preliminary design of a whole-arm manipulation system (WAMS). *IEEE international conference on robotics and automation, ICRA*. (pp. 254–260). New York, NY: IEEE.

Siciliano, B., Sciavicco, L., Villani, L., & Oriolo, G. (2009). *Robotics modelling, planning and control*. Springer-Verlag Advanced Textbooks in Control and Signal Processing.

Singh, L., Stephanou, H., & Wen, J. (1996). Real-time robot motion control with circulatory fields. *IEEE international conference on robotics and automation, ICRA* (pp. 2737–2742). New York, NY: IEEE.

Takegaki, M., & Arimoto, S. (1981a). A new feedback method for dynamic control of manipulators. *ASME Journal of Dynamic Systems Measurement and Control*, *103*, 119–125.

Takegaki, M., & Arimoto, S. (1981b). A new feedback method for dynamic control of manipulators, ASME. *Journal of Dynamic Systems, Measurement, and Control, 103*, 119–125.

Tarn, T., Bejczy, A., Isidori, A., & Chen, Y. (1984). Nonlinear feedback in robot arm control. *IEEE conference on decision and control* (pp. 736–751). New York, NY: IEEE.

Versace, J. (1971). A review of the severity index. *Car crash conference* (pp. 771–796). Warrendale, PA: Society of Automotive Engineers.

Wojtara, T., Uchihara, M., Murayama, H., Shimoda, S., Sakai, S., Fujimoto, H., & Kimura, H. (2009). Human-robot collaboration in precise positioning of a three-dimensional object. *Automatica, 45*, 333–342.

Yamada, Y., Hirasawa, Y., Huang, S., Umetani, Y., & Suita, K. (1997). Human-robot contact in the safeguarding space. *IEEE/ASME Transactions on Mechatronics, 2*, 230–236.

Zanchettin, A., Lacevic, B., & Rocco, P. (2012). A novel passivity-based control law for safe human-robot coexistence. *IEEE/RSJ international conference on intelligent robots and systems, IROS* (pp. 2276–2281). New York, NY: IEEE.

Zinn, M., Khatib, O., Roth, B., & Salisbury, J. (2004). Playing it safe [human-friendly robots]. *Robotics Automation Magazine, IEEE, 11*, 12–21.